

**GPS Observations of Fault Afterslip and Upper Crustal  
Deformation Following the Northridge Earthquake**

Andrea Donnellan

Gregory A. Lyzenga\*

*Jet Propulsion Laboratory, California Institute of Technology, Pasadena, California*

Address correspondence to:

Andrea Donnellan  
Mail Stop 238-600  
4800 Oak Grove Drive  
Pasadena, CA 91109-8099

Phone: 818-354-4737

Fax: 818-393-4965

submitted: 8/4/97

revised: 12/17/97

\*Also at Harvey Mudd College, Claremont, CA

## Abstract

Global Positioning System (GPS) observations indicate that significant aseismic deformation occurred in the year following the January 17, 1994 Northridge earthquake. The postseismic station observations show the same sense of motions as observed in the co-seismic offsets. As compared with the coseismic displacements, the far-field post-seismic motions (1–2 fault dimensions away) are proportionally larger than those seen in the near field. The post-seismic data are best modeled with two faults: one on the rupture plane and one located in the shallow crust. The upper crustal fault may represent an actual fault or may be indicative of viscous relaxation occurring in the upper crust. The afterslip and/or relaxation accounts for about  $3.7 \times 10^{18}$  N•m or 28% that of the mainshock moment release. We expect that the moment release due to the afterslip and relaxation effectively reduce the earthquake hazard locally. It is not clear from this study how the postseismic deformation loads the surrounding faults or alters the state of stress on those faults.

## Background

The magnitude 6.7 Northridge earthquake occurred on the morning of January 17, 1994 [Jones *et al.*, 1994]. This thrust event ruptured a south-dipping ramp from a hypocentral depth of ~20 km in the central part of the San Fernando Valley, breaking upward and northward towards the mountains to a minimum depth of ~5 km [Hauksson *et al.*, 1995]. The rupture was ~18 km in lateral extent and the average slip on the fault was estimated to be about 101–130 cm [Wald *et al.*, 1996].

The Northridge earthquake occurred near the southeastern margin of the Ventura basin (Figure 1). The basin is marked by an extraordinarily thick sedimentary section [Luyendyk and Hornafius, 1987; Norris and Webb, 1990], which is extensively folded near the surface. East-west striking thrust faults bound the basin and dip away from the central trough [Yeats, 1983].

## Observations

Global Positioning System (GPS) data have been collected in the region just to the west of the epicenter of the Northridge earthquake since 1987 as part of a geodetic study of the Ventura basin [Donnellan *et al.*, 1993a; Donnellan *et al.*, 1993b] (Figure 1). In the one month following the earthquake, the network was reoccupied and two additional stations were established near the source of the earthquake: one at California State University Northridge (CSUN) and another in the Granada Hills just south of the Santa Susana Mountains and near the upper terminus of the rupture plane (LNCH). The stations were reoccupied for 2–3 days at approximately 6 month intervals through the summer of 1995 (Figure 2). A continuously operating station (OATT) was installed on Oat Mountain near one of the original Ventura basin network monuments and tied into the original mark in 1996.

The GPS data were processed using the GIPSY/OASIS II software and JPL precise orbits and clocks [Zumberge *et al.*, 1997]. Orbits and clocks were fixed and large outliers in the raw data were removed in bias-free solutions for each day. We then performed ambiguity resolution on the each days observed network. The individual station covariance files for each day were then combined into one velocity estimation. The few large outliers

in station position were removed from the final solution. The  $\chi^2/\text{dof}$  for the combined solution was nearly 20 so we scaled the  $1\sigma$  velocity errors by 4.5 so that  $\chi^2/\text{dof}=1$ .

## Post-Seismic Results

Determination of the post-seismic deformation field is dependent on a clear understanding of the pre-seismic velocities because any post-seismic transients appear superposed over the background velocity field. We examined the data in several ways in order to understand the post-seismic velocity field.

For this study we opted to use the observed post-seismic velocities minus the contribution of shear from the San Andreas and other strike slip faults in southern California (Tables 1 and 2). We used two general features of the pre-Northridge velocity field to justify this approach. First, the pre-Northridge velocity between the site Castro Peak (CATO) and LaCumbre Peak (LACU/RCAG) is well determined and is essentially zero ( $0.0 \pm 0.6$  mm/yr in east,  $0.2 \pm 0.5$  mm/yr in north [Dong, personal communication]). We, therefore, computed the shear velocities of the stations relative to LACU/RCAG and removed them from the observed velocities relative to LACU/RCAG. Second, the region south of the Ventura basin has shown block-like behavior for the past 100 years after removal of shear contribution from the San Andreas and other strike-slip faults [Donnellan *et al.*, 1993a,b]. The Northridge earthquake occurred within this block and for this study we model the post-Northridge velocities of the stations within the same block. A benefit of this method is that we did not need to interpolate the velocities for either CSUN or LNCH. Velocities of stations to the north of the basin do not depart substantially from the pre-Northridge velocities and are not on the rigid block, so we do not include them in the

modeling. It is possible that the Northridge earthquake triggered motion on other basin bounding faults and modeling those faults is beyond the scope of this paper. Additional observations collected over a longer time span are required to determine whether the shortening rate across the basin changed following the Northridge earthquake.

Rigorous propagation of errors associated with the shear velocity field model is not possible in the absence of hard uncertainties for the shear model. However, as a worst-case estimate, we compared a model of San Andreas-only shear with one incorporating all of the principal strike slip faults of the region. The results differ by about 2 mm/yr in the east component and 0.5 mm in the north across the network. The vertical error budget is unaffected by the shear model. Although it is possible that the horizontal errors may actually be somewhat larger than reported, the effect of this on the fault inversion parameters would be negligible while the errors on the parameters would be slightly larger.

The residual velocity field is comparable to a residual velocity field in which the pre-Northridge velocities are subtracted from the post-Northridge velocities. However, there were large east-west biases on the order of several mm/yr for the various velocity solutions that we examined, due in part to various treatments of offsets due to the Landers earthquake. We examined the data in several ways in order to understand the post-seismic deformation. We did not use the velocity field of *Shen et al.* [1996a] because that solution includes data collected after the earthquake, and while the solution accounts for co-seismic offsets, it is potentially biased by post-seismic transients. We compared the post-seismic data (Table 1) to a velocity field computed for the region that included only GPS data collected prior to the Northridge earthquake [*Dong*, personal communication]. The stations

LNCH and CSUN did not exist prior to the earthquake and therefore the pre-earthquake velocities for those stations were interpolated from nearby stations. HAP2 also has a poorly determined velocity because its first epoch of occupation was in 1992. In addition the last two epochs of data for the area span the 1992 Landers earthquake, which was large enough to cause differential motions at the level of up to a few mm/yr between stations within the Ventura basin network. For this reason the errors on the pre-Northridge velocity field are large and the resultant errors for the post-seismic residual velocity field are correspondingly large.

For the present study we assume that the vertical velocities were zero prior to the earthquake, since the vertical velocities determined from early campaign-style GPS measurements are of small magnitude and not distinguishable from null motion. In contrast, the vertical components are among the best determined post-seismic motions, primarily because of their comparatively large amplitude. They indicate uplift over the rupture plane similar in distribution to, but smaller than, the co-seismic results [*Hudnut et al.*, 1996]. The peak measured uplift is 12 cm above the upper edge of the rupture plane in the Granada Hills (LNCH; Figure 3). The post-seismic pattern of the horizontal motions is also similar to the co-seismic pattern, with stations to the north and south of the rupture moving toward the rupture plane, and stations east and west moving away from the rupture.

For the purposes of modeling the data we computed steady post-seismic velocities rather than displacements for the stations. The reason for this is twofold. First, not all stations were observed at the same times, including late and early in the time series, and

therefore the displacements for each site would cover a different time period (Figure 2). Second, by calculating velocities we were able to incorporate all of the data collected for each station, and were thus, not reliant on just the first and last occupations, which could possibly contain an error in position due to blunder. We expect that the residual velocities, which are a best fit to 1.5 years of data, adequately reflect the post-seismic motions, although in actuality the velocities were faster early in the post-Northridge time series and slower late in the time series.

The observable post-seismic transients decay with time, with most of the motion occurring within the first year after the earthquake (Figure 3). The horizontal and vertical post-seismic motions, at stations where they are significant, can be fit fairly well by an exponential time dependence ( $y = a(1 - \exp(-b(t - t_0))) + c$ ) with a characteristic decay time in the range 0.3–1.4 years. Both the horizontal and vertical motions can be fit equally well (or perhaps slightly better) by a logarithmic function ( $y = a \ln(t - t_0) + b$ ). Exponential decay characterizes relaxation of a Maxwell viscoelastic solid, while fault afterslip may be expected to obey a logarithmic law [Marone *et al.*, 1991]. These results imply that we are unable to distinguish between afterslip and relaxation mechanisms. The models presented in this paper suggest that both processes may have occurred following the earthquake.

### Northridge Aftershocks

We tested whether aftershocks could account for the post-seismic motions prior to modeling the GPS data. We used first motion locations and mechanisms for 65 aftershocks determined by Hauksson *et al.* [1995] for the time period January 18, 1994 through June 15, 1994 ranging in magnitude from 4.0 to 5.2. We excluded aftershocks

that occurred on January 17, 1994, the day of the earthquake, and also a M 5.1 aftershock that occurred on January 29, 1994. We excluded the aftershocks from the day of the earthquake because we did not collect any GPS data on that day, hence our results do not include post-seismic motion immediately following the earthquake. We also excluded the aftershock of January 29, 1994 because it was very shallow and affected the GPS results for at least the station on Oat Mountain (OATT), which was displaced 4 cm to the south [Donnellan and Webb, manuscript submitted]. We have excluded the post-seismic observations at SAFE/OATT collected before 29 January, 1994 in the calculation of the post-seismic velocity and therefore do not include the aftershock in the comparison with the GPS results.

We can account for no more than 10% of the post-seismic motion with aftershocks. We used the moment/magnitude relation  $M_w = 2/3 \cdot \log(M) - 6.7$  and  $M = \mu \cdot \Delta S \cdot A$ , where  $M$  is moment,  $M_w$  moment magnitude,  $\mu$  rigidity,  $\Delta S$  fault slip, and  $A$  fault area [Hanks and Kanamori, 1979]. For this exercise the local magnitudes are comparable to moment magnitudes. We assumed a depth dependent rigidity based on the tomographic velocity model of Haase *et al.* [1996]. The S-wave velocities, and thus the rigidity, for the region are low (1.6–2.9 km/s) [Haase *et al.*, 1996] permitting a larger fault area or slip for a given magnitude. One might argue, however, that the aftershock ruptures occurred on low-rigidity surfaces. We also tested for displacements with a rigidity of 4 GPa, which is the lower limit for sandstone [Turcotte and Schubert, 1982]. This was to provide an upper limit on the post-seismic motion due to aftershocks. Because the Northridge region is composed of loosely consolidated marine sediments a low rigidity is reasonable. Even

these maximum displacements are not enough to account for the observed post-seismic motions.

After estimating the fault area and slip for each aftershock, we calculated the surface displacements by using point dislocations in an elastic half-space [Okada, 1985]. The predicted surface displacements from the aftershocks show generally the same sense of motion as the GPS observations (Figure 4). The magnitudes of the motions are less than 10% those of the measured motions, suggesting that at least 90% of the post-seismic motion has occurred aseismically. Given our low estimates of the rigidity it is likely that more than 90% of the post-seismic motion is aseismic. Apparently, however, the aftershocks are responding to the same stress field responsible for the aseismic motions, since the sense of motion is the same.

## Modeling

We formulated a series of models in an effort to explain the observed pattern of surface deformation. Forward finite element models and inverse dislocation solutions were employed to examine complementary scenarios of anelastic crustal deformation and elastic afterslip. We begin by eliminating those models that clearly fail to reproduce the observed motions and then proceed to discuss candidate models that are generally consistent with observation.

In the series of finite element models, a viscoelastic rheology is invoked for parts of the crust and upper mantle, in order to accommodate long-term plastic strain during the postseismic and interseismic periods. The baseline model is a simplified two-dimensional layered structure consisting of elastic crust down to a depth of 15 km, based on the

approximate lower depth limit of California seismicity [Webb and Kanamori, 1975]. A viscoelastic lower crust is assumed from 15 km to a Moho depth of 35 km. The rheology of the deepest layers below 35 km does not strongly influence the present results. It is assumed to have a nominal Maxwell rheology roughly approximating the nonlinear flow law of olivine [Poirier, 1995] and having a relaxation time of 100 years.

### **Lower Crustal Relaxation**

The most conventional viscoelastic model of postseismic relaxation simply relies on the flow of lower crustal (and to a lesser degree, mantle) material to explain transient deformation. Here, this layer is assigned a Maxwell viscoelastic rheology with a relaxation time of 300 years. This time constant is longer than is typically assumed for southern California models, but it is believed to be appropriate for this region of cool crustal downwelling [Humphreys and Clayton, 1990] and low crustal heat flow [DeRito *et al.*, 1989]. While the lower crustal viscosity is not very strongly constrained by geodesy, pre-earthquake strain profiles favor a relatively cold and stiff lower crust in this region with a relaxation time on the order of a few hundred years [work in progress]. Such a long characteristic relaxation time is inadequate to explain the kind of short-term transient motions observed after the Northridge earthquake. In addition to predicting the wrong time dependence, lower crustal viscoelastic relaxation produces horizontal motions that are in the same sense as the observed motions, but the vertical motions are in the opposite sense, particularly over the fault plane. The observations indicate uplift over the fault plane following the earthquake while these models predict downward motion for that region.

Non-Newtonian rheology, in which the effective viscosity (and resulting relaxation time) would be greatly reduced by the coseismic stress increment near the fault, may be invoked as means of explaining rapid transient relaxation. This was achieved in the finite element models by assigning the lower crustal layer a power-law rheology in which strain rate varies as the third power ( $n=3$ ) of the ambient stress. Although such rheological descriptions of crustal rocks may be derived from laboratory tests [Poirier, 1995], the assignment of a specific flow law here is largely empirical. We selected the particular stress-dependent viscosity to provide about a 1 year relaxation time scale for stresses on the order of the coseismic stress drop. In this model, the effective viscosity (and relaxation time) decrease as the square of the crustal stress, so that at typical interseismic strain rates and stresses the effective Newtonian relaxation time is increased to about 30 years, still an order of magnitude lower than expected based on modeling of pre-Northridge data. In this case the horizontal motions are also compatible with the observed motions, and the predicted vertical motions still have the opposite sense of those observed. The nonlinear model is essentially the same as the linear model except that the effective viscosity is lower. These results suggest that while lower crustal relaxation may play a role later in the earthquake cycle some other process controls the deformation in the few years following the earthquake.

### **Fault Afterslip**

As mentioned above, the rate of decay for the post-seismic motion can be fit by a logarithmic function indicative of fault afterslip. We performed a suite of inversions to test for this mechanism. The results indicate that fault afterslip very likely occurred following

the earthquake. To perform the inversions we used a downhill search, or residual minimization algorithm, for elastic fault parameters. We tested for afterslip on the rupture plane, as well as on the downdip and updip extensions of the fault. We also tested for afterslip in locations other than the fault plane. While the data are not detailed enough to provide a unique solution, the inversions do provide insight into the processes that may have occurred following the earthquake.

The residual-minimization procedure is based upon the downhill simplex simulated annealing algorithm described by Press et al. [1988]. A  $\chi^2$  goodness of fit objective function is formed from the horizontal and/or vertical components of displacement at each geodetic observation point and their respective measurement uncertainties. Function evaluations are based upon the elastostatic solutions for rectangular half-space dislocations given by Okada [1985]. Since the function may have a very complex configuration of local minima, the simulated annealing strategy is employed as a means of locating a global minimum. Since the technique is iterative, the uniqueness and quality of the resulting solution is assessed numerically, by differentiation of the objective function.

The best model that allows for slip on one plane prefers the slip to be located above the upper portion of the rupture zone (Table 4; Figures 5 and 6). The data do not permit slip on the downdip extension. If we restrict the slip such that it occurs only on the downdip extension of the fault, the misfit of the residuals ( $\chi^2/\text{dof}$ ) is large ( $\sim 5$ ). If we free up various parameters the slip is either located above 18 km or the fit is unrealistic (e.g. extremely large slip on an extremely narrow fault). Similar results occur for slip on the updip extension of the fault; the afterslip does not extend updip from the rupture plane.

The inversion requires about 15 cm of left-lateral oblique slip with a rake of about  $15^\circ$ . The slip is about 12% of the mainshock slip and the potency, or moment, is about 4% that of the coseismic model of *Wald et al.* [1996]. While the one-fault model fits the near-field data fairly well, it does not fit the farther field results particularly well.

### **Deformation of the Upper Crust**

The one-fault models do not agree well with the observed far-field motion. In a second set of inversions we solved for an auxiliary fault while fixing and freeing various parameters. This heuristic approach was dictated by the limited degrees of freedom and data strength afforded by the sparse data set. In each of these inversions nearly pure thrust afterslip occurs on one fault that fits the entire mainshock rupture plane. No slip extends above or below the rupture plane and with the addition of a second fault the slip does not extend beyond the rupture plane laterally (Figures 7 and 8). We present the best model in this paper, however it should be taken as broadly representative of the possible post-seismic mechanisms. We experimented with dozens of models by varying the initial values and fixed parameters. Afterslip on the main fault and additional slip on an auxiliary fault emerge as the best fitting models.

The auxiliary fault tends to be located west of and bounds the western extent of the afterslip zone, with a dip similar to that of the mainshock plane. This plane is located much shallower in the crust and extends to the surface from about 11 km. Additionally, the slip is about one tenth of the slip on the afterslip plane and shows nearly equivalent amounts of left-lateral and thrust motion. The two-fault model fits both the near-field and farther field horizontal and vertical motions (Figures 7 and 9).

The results suggest a quasi-ductile flow in the upper crust as a result of the Northridge earthquake. The auxiliary fault does not correspond to any mapped fault, but may rather be indicative of general deformation of the upper crust as a result of the Northridge earthquake. This “fault”, which is more likely representative of broad deformation in the upper crust coincides with shallow aftershocks that are also interpreted as deformation of a quasi-elastic material [Unruh, *et al.*, in press]. Unfortunately there are not adequate data to test for similar deformation to the east of and above the rupture, though the Jet Propulsion Laboratory continuous station (JPLM), located about 30 km east of the rupture, shows anomalous eastward motion following the earthquake, which may mirror the motion of the stations west of the rupture zone [Heflin *et al.*, 1997].

When we include post-seismic motion from JPLM in the inversions in a two-fault model the first fault is located directly on the rupture plane and a second fault is found in the shallow crust. Although the model is non-unique, in every case where we solve for two faults, one fault is always located on the rupture plane, and one fault is located in the shallow crust. The position of the shallow fault varies from inversion to inversion, suggesting broad distributed deformation rather than motion on one discrete fault. This broad shallow deformation is required to fit the observations in the far-field. While a model of lower rather than upper crustal deformation fits the horizontal far-field motions the vertical motions are in the opposite sense of those observed. The two-fault model fits the data better than the one-fault model with a confidence of 70% according to an f-test. There is a 30% chance that the improvement in fit is due to random chance, but since for

the two fault model one fault is located directly on the rupture plane where we would expect afterslip the two-fault model seems qualitatively preferable as well.

We investigated the predicted effects of a soft upper crust in an otherwise homogeneous half-space by first running forward finite element models for a two-dimensional thrust fault overlain by a soft upper crust of varying thickness. In these models the relaxation time is nominally one year and the upper layer thickness is 5 km. Subsequently the finite element model surface displacements were inverted for an effective elastic fault source, a proxy for the ductile upper crust [Lyzenga *et al.*, manuscript in preparation]. By doing so, we are more easily able to look at the 3-dimensional effects of viscous deformation in the upper crust. In the 2-dimensional finite element models the uplift profile is narrower and higher than an afterslip model predicts, similar to the observed results. In each of the inversions of the finite element models the effective fault is located above the actual fault plane in the hanging wall block with a slightly lower dip. The effects are more pronounced for a thicker soft layer. These trial models suggest that inversions of the real data that result in a fault in the shallow crust such as the one-fault model may be reflective of ductile upper crustal deformation rather than actual slip on a shallow fault. Unfortunately the data are too sparse to conclusively test for relaxation of the upper crust.

The correct rheology to describe the behavior of the marine sedimentary deposits comprising the upper few kilometers of the study region must be complex. While in the current study we approximate its behavior as Maxwell-Newtonian viscoelastic, it is clear that this behavior must be a poor approximation at low stress levels. A more plausible

description at low stress loads might be an elastic-plastic rheology. In such a case, earthquake-generated stress levels on the order of bars could be sufficient to trigger plastic quasi-viscous deformation. It is somewhat problematic that this is comparable the stresses associated with topography a few hundred meters in amplitude, which appears to be supported for long periods in parts of the Ventura basin region. Since the inferred location of the quasi-ductile deformation is with the basin proper, where there is minimal topography, there may be a strong contrast between the plastic properties of the uplifted blocks and the younger alluvial basin deposits. This possible problem with the quasi-ductile model will require more observations to resolve.

Listric faults in horizontally layered elastic media can produce geodetic displacements that yield half-space inversions with depths shallower than the true depth [Du et al., 1994]. This effect is unlikely, however, to explain much of the shallow post-seismic deformation inferred from this study. For the comparatively steep dip of the Northridge fault plane, reasonable elastic modulus variations do not move the apparent coseismic fault plane by more than a few kilometers. In contrast, inversions of the post-seismic geodetic data for one fault plane result in a fault displaced upward on the order of about 10 km. Furthermore, the coseismic rupture plane inferred from geodetic observations is only a few km above the plane inferred from seismological observations. If the postseismic offset is due strictly to elastic layering it should be on the same order as the coseismic results.

The results from the two-dimensional models may also explain why inversions of the coseismic data result in a fault displaced upward from the aftershock zone when the

fault is not constrained to the aftershock zone [e.g. *Hudnut et al.*, 1996]. *Shen et al.* [1996b] could not fit the GPS data with a single fault through the aftershocks by using either a homogeneous or layered elastic half-space. They were able to fit the data best if they included an additional north-dipping fault located above the main rupture. The conjugate of the upper fault is similar in dip and location to the shallow fault in our inversions. The GPS data used in these studies were collected up to a month after the Northridge earthquake and therefore the reported coseismic offsets include early postseismic deformation as well.

## Implications

The post-seismic observations indicate that different processes dominate before and after the Northridge earthquake. Pre-Northridge geodetic observations are best explained by relaxation of a stiff viscoelastic lower crust and an elastically heterogeneous upper crust. Relaxation of the lower crust causes vertical motions that are opposite in sense from those observed in the immediate postseismic period. Furthermore, the predicted rates of motion from this mechanism are an order of magnitude smaller than those observed. Therefore, the presence of a stiff viscoelastic lower crust is not inconsistent with the post-earthquake observations, but is not the process dominating the post-seismic deformation.

Conversely, the post-seismic mechanisms that we propose here do not apparently play a significant role late in the earthquake cycle. Our observations indicate a post-seismic decay time constant of about  $<1$  year, implying that essentially all of the shallow post-seismic deformation should have occurred within 5 years after the earthquake. Our relaxation models assume a simple exponential decay rate and only additional observations

will verify if this is appropriate. Additional observations will also indicate how other faults near Northridge and the Ventura basin have been affected by the Northridge earthquake.

The post-seismic moment release over the two-year period following the earthquake is about  $3.7 \times 10^{18}$  N•m or 28% that of the mainshock moment release (potency of  $0.13 \text{ km}^3$ ). This follows from the inference of about 22 cm/yr of post-seismic slip occurring on the rupture plane and about 5 cm/yr of equivalent displacement occurring through deformation of an auxiliary plane in the upper crust for the two years following the earthquake. The auxiliary plane may actually represent deformation of a soft upper crust and most likely would occur through folding. Folds are pervasive in the Northridge and Ventura basin region [Yeats, 1983] as are bedding plane faults in the Oak Ridge [Rockwell, personal communication].

Inversions for co-seismic fault slip have been carried out using strong motion, teleseismic, and geodetic data [Wald *et al.*, 1996]. Those inversions that include geodetic data predict a 10–30% larger average slip for the Northridge earthquake than those that include only seismic data. Observations of postseismic release on the order of 10–20% of the coseismic are not unusual following other earthquakes of comparable and larger size [e.g. Argus and Lyzenga, 1994; Barrientos *et al.*, 1992; Savage and Lisowski, 1995; Lisowski *et al.*, 1990; Shen *et al.*, 1994]. It is possible that the geodetic data (particularly the leveling data), which were collected up to 8 months after the earthquake, reflect post-seismic as well as co-seismic motions. This would result in a higher estimate of slip than from a solution using only seismic data. The slip discrepancy for inversions that include

the leveling data is generally consistent with the post-seismic slip that we infer from the GPS observations.

These model results also suggest that a plastic upper crustal rheology has consequences observable in the (nominally) coseismic geodetic data. Published inversions for coseismic fault slip constrain the modeled fault to coincide with the aftershock zone [Wald *et al.*, 1996]. However, when the GPS geodetic data are inverted for fault slip, location and orientation in an isotropic elastic half-space, the preferred fault plane is located 2–3 km above the aftershock zone [Hudnut *et al.*, 1996] or a second fault in the shallow crust is required [Shen *et al.*, 1996b]. Since these geodetic data were acquired over a period of weeks following the main shock, they are likely to be partially contaminated by postseismic deformation.

The post-seismic mechanisms that we propose may explain why the upper portion of the crust can be well described by thin-skinned tectonic models, while the major recent earthquakes tend to rupture on moderately steeply dipping faults extending from the lower crust as described by thick-skinned tectonic models. It may be that thick-skinned processes dominate for the moderate to large earthquakes and that thin-skinned processes occur following these events as a means of redistributing stress. Thin-skinned tectonics is characterized by low angle faults that terminate in folds [Suppe and Medwedeff, 1990]. The deformation in the soft upper crust may result from folding of the sediments and slip on bedding plane faults in regions where the stress concentrations are greatest following earthquakes. Our best fit model requires deformation of the upper crust as well as afterslip on the main rupture plane. Similar results have been obtained in analysis of post-seismic

geodetic data following the Loma Prieta earthquake [Bürgmann *et al.*, 1997]. The best fitting model for the Loma Prieta post-seismic data requires two faults, with one located in the aftershock zone and one located in the shallow crust.

Based on the inferred decay rate, up 30% of the mainshock moment release is expected to occur quietly in the years following the earthquake. This is the moment equivalent of a magnitude 5.8–6.3 earthquake (given a rigidity range of about 4–29 GPa). If aseismic deformation commonly occurs following moderate to large earthquakes in southern California, earthquake potential and hazard estimated on the basis of regional strain accumulation may require reassessment. A 30% near-field reduction of seismic moment release is not large enough alone, however, to rule out the possibility of either more frequent moderate earthquakes than historically observed or larger Mw 7.1–7.5 earthquakes in the Los Angeles region [Dolan *et al.*, 1995]. We account for aseismic deformation in the near-field of a moderate earthquake. Other aseismic processes may occur, which would further reduce the percentage of seismic moment release in southern California.

## Acknowledgments

We gratefully acknowledge the invaluable assistance of M. B. Heflin, M. Watkins, D. Jefferson, F. Webb, D. Dong, J. Parker, and W. Panero in the analysis and modeling of the geodetic data. We are grateful for the help of D. Dager, G. Franklin, M. Glasscoe, M. Gurnis, K. Hurst, A. Mikolajcik, and M. Smith in the field acquisition of data. This work was carried out at the Jet Propulsion Laboratory, California Institute of Technology, under contract with NASA. Support was also provided by the U.S. Geological Survey

and National Science Foundation through the National Earthquake Hazards Reduction Program (NEHRP) and the Southern California Earthquake Center (SCEC). SCEC is funded by NSF Cooperative Agreement EAR-8920136 and USGS Cooperative Agreements 14-08-0001-A0899 and 1434-HQ-97AG01718. The SCEC contribution number for this paper is 398.

## References

- Argus, D.F., G.A. Lyzenga, Site velocities before and after the Loma Prieta and Gulf of Alaska earthquakes determined from VLBI, *Geophys. Res. Lett.*, **21**, 333–336, 1994.
- Barrientos, S.E., G. Plafker, E. Lorca, Post-seismic coastal uplift in southern Chile, *Geophys. Res. Lett.*, **19**, 701–704, 1992.
- Bürgmann, R., P. Segall, M. Lisowski, and J. Svarc, Postseismic strain following the 1989 Loma Prieta earthquake from GPS and leveling measurements, *J. Geophys. Res.*, **102**, 4933–4955, 1997.
- DeRito, R.F., A.H. Lachenbruch, T.H. Moses, and R.J. Munroe, Heat flow and thermotectonic problems of the central Ventura basin, southern California, *J. Geophys. Res.*, **94**, 681–699, 1989.
- Dolan, J.F., K. Sieh, T.K. Rockwell, R.S. Yeats, J. Shaw, J. Suppe, G.J. Huftile, and E.M. Gath, Prospects for larger or more frequent earthquakes in the Los Angeles metropolitan region, *Science*, **267**, 199–205, 1995.
- Donnellan, A., B. H. Hager, and R. W. King, Discrepancy Between Geologic and Geodetic Deformation Rates in the Ventura Basin, *Nature*, **366**, 333–336, 1993a.

- Donnellan, A., B. H. Hager, R. W. King, and T. A. Herring, Geodetic Measurement of Deformation in the Ventura Basin Region, Southern California, *J. Geophys. Res.*, **98**, 21,727–21,739, 1993b.
- Donnellan, A., and F.H. Webb, Geodetic observations of the M 5.1 January 29, 1994 Northridge aftershock, *Geophys. Res. Lett.*, manuscript submitted.
- Y. Du, P. Segall, H. Gao, Dislocations in inhomogeneous media via a moduli perturbation approach: General formulation and two-dimensional solutions, *J. Geophys. Res.*, **99**, 13767–13779, 1994.
- Haase, J.S., E. Hauksson, F. Vernon, and A. Edelman, Modeling of ground motion from a 1994 Northridge aftershock using a tomographic velocity model of the Los Angeles basin, *Bull. Seism. Soc. Am.*, **86**, S156–S167, 1996.
- Hanks, T. C., and H. Kanamori, A moment magnitude scale, *J. Geophys. Res.*, **84**, 2348–2350, 1979.
- Hauksson, E., L.M. Jones, K. Hutton, The 1994 Northridge earthquake sequence in California—seismological and tectonic aspects, *J. Geophys. Res.*, **100**, 12,335–12,355, 1995.
- Heflin, M.B., D. Darger, D. Dong, A. Donnellan, K. Hurst, D. Jefferson, G. Lyzenga, M. Watkins, F. Webb, and J. Zumberge, Transient observed at JPLM after the Northridge Earthquake, *EOS Trans. Am. Geophys. Un. Suppl.*, **S209**, 1997.
- Hudnut, K. W., Z. Shen, M. Murray, S. McClusky, R. King, T. Herring, B. Hager, Y. Feng, P. Fang, A. Donnellan and Y. Bock, Co-seismic displacements of the 1994 Northridge, California, earthquake, *Bull. Seism. Soc. Am.*, **86**, S19–S36, 1996.
- Humphreys, E.D., R.W. Clayton, Tomographic image of the southern California mantle, *J. Geophys. Res.*, **95**, 19725–19746, 1990.
- Donnellan and Lyzenga submitted to *J. Geophys. Res.* 8/4/97

- Jones, L., K. Aki, M. Celebi, A. Donnellan, J. Hall, R. Harris, E. Hauksson, T. Heaton, S. Hough, K. Hudnut, K. Hutton, M. Johnston, W. Joyner, H. Kanamori, G. Marshall, A. Michael, J. Mori, M. Murray, D. Ponti, P. Reasenberg, D. Schwartz, L. Seeber, A. Shakal, R. Simpson, H. Thio, M. Todorovska, M. Trifunovic, D. Wald, and M. L. Zobak, The magnitude 6.7 Northridge, California, earthquake of 17 January 1994, *Science*, **266**, 389–397, 1994.
- Lisowski, M., W.H. Prescott, J.C. Savage, and M.J. Johnston, Geodetic estimate of coseismic slip during the 1989 Loma Prieta, California, earthquake, *Geophys. Res. Lett.*, **17**, 1437–1440, 1990.
- Luyendyk, B.P. and J. S. Hornafius, Neogene crustal rotations, fault slip, and basin development in southern California, in *Cenozoic Basin Development of Coastal California*, **6**, R. V. Ingersoll and W. G. Ernst, Eds., Prentice Hall, Inc., Englewood Cliffs, NJ, pp. 259–283, 1987.
- Marone, C.J., C.H. Scholz, R. Bilham, On the mechanics of earthquake afterslip, *J. Geophys. Res.*, **96**, 8441–8452, 1991.
- Norris, R.M. and R.W. Webb, *Geology of California*, John Wiley & Sons, Inc., New York, 2nd ed., 1990.
- Okada, Y., Surface Deformation Due to Shear and Tensile Faults in a Half-Space, *Bull. Seism. Soc. Am.*, **75**, 1135–1154, 1985.
- Poirier, J. P., in *Mineral physics and crystallography: a handbook of physical constants*, T. J. Ahrens, Ed., American Geophysical Union, Washington, DC, pp. 237–247, 1995.

- Press, W.H., B.P. Flannery, S.A. Teukolsky, and W.T. Vetterling, Numerical Recipes in C, Cambridge University Press, New York, 733pp., 1988.
- Savage, J.C., and M. Lisowski, Changes in long-term extension rates associated with the Morgan Hill and Loma Prieta earthquakes in California, *Geophys. Res. Lett.*, **22**, 759–762, 1995.
- Shen, Z., D.D. Jackson, and B.X. Ge, Crustal deformation across and beyond the Los Angeles basin from geodetic measurements, *J. Geophys. Res.*, **101**, 27,957–27,980, 1996a.
- Shen, Z., B.X. Ge, D.D. Jackson, D. Potter, M. Cline, and L. Sung, Northridge earthquake rupture models based on the Global Positioning System measurements, *Bull. Seism. Soc. Am.*, **86**, S37–S48, 1996b.
- Shen, Z.K., D.D. Jackson, Y.J. Feng, M. Cline, M. Kim, P. Fang, and Y. Bock, Post-seismic deformation following the Landers earthquake, California, 28 June 1992, *Bull. Seism. Soc. Am.*, **84**, 780–791, 1994.
- Suppe, J. and D.A. Medwedeff, Geometry and kinematics of fault-propagation folding, *Eclogae, Geol. Helv.*, **83**, 409–454, 1990.
- Turcotte, D.L., and G. Schubert, Geodynamics: Applications of Continuum Physics to Geological Problems, John Wiles & Sons, Inc., New York, 450pp., 1982.
- Unruh, J.R., R.J. Twiss, and E. Hauksson, Kinematics of post-seismic relaxation from aftershock focal mechanisms of the 1994 Northridge, California earthquake, *J. Geophys. Res.*, in press.
- Wald, D.J., T.H. Heaton, K.W. Hudnut, The slip history of the 1994 Northridge, California, earthquake determined from strong-motion, teleseismic, GPS, and leveling data, *Bull. Seism. Soc. Am.*, **86**, S49–S70, 1996.

- Webb, T.H. and H. Kanamori, Earthquake focal mechanisms in the eastern Transverse Ranges and San Emigdio Mountains, southern California and evidence for and regional décollement, *Bull. Seism. Soc. Am.*, **75**, 737–757, 1975.
- Yeats, R.S., Large-scale Quaternary detachments in the Ventura basin, southern California, *J. Geophys. Res.*, **88**, 569–583, 1983.
- Zumberge, J.F., M.B. Heflin, D.C. Jefferson, M.M. Watkins, and F.H. Webb, Precise point positioning for the efficient and robust analysis of GPS data from large networks, *J. Geophys. Res.*, **102**, 5005–5017, 1997.

Station	Latitude	Longitude	East (mm/yr)	North (mm/yr)	Vertical (mm/yr)
CATO	34.086	-118.786	3.7±2.5	6.6±2.6	-0.4± 9.9
CSUN	34.244	-118.531	-0.9±8.3	-4.4±4.0	15.4±11.8
HAP2	34.328	-118.877	-6.6±2.8	4.4±3.0	-2.4±19.4
HAPY	34.358	-118.850	-11.4±7.7	-2.3±5.0	-2.6±22.3
LNCH	34.301	-118.510	15.5±2.2	-8.2±2.4	62.8±11.8
OATT	34.330	-118.601	1.0±2.0	1.5±2.1	20.8± 6.3
SAFE	34.330	-118.601	-2.9±1.9	1.2±2.0	23.4± 4.4

Table 1: Post-Northridge observed velocities relative to RCAG. Errors are scaled  $1\sigma$ .

Fault	Longitude	Latitude	Strike (deg)	Depth (km)	Length (km)	Slip (mm/yr)
<i>San Andreas</i>	-121.217	36.600	318	10	$\infty$	34
	-120.583	35.967	321	1	92	34
	-119.383	34.917	317	25	160	34
	-119.383	34.917	106	25	97	34
	-118.367	34.667	118	25	116	34
	-117.250	34.167	107	25	77	19
	-116.490	33.990	133	15	$\infty$	19
<i>Garlock</i>	-118.933	34.817	57	10	160	-10
<i>Elsinore</i>	-117.667	33.900	130	15	$\infty$	5
<i>San Jacinto</i>	-117.533	34.300	132	10	$\infty$	10
<i>Newport-Inglewood</i>	-118.278	34.000	142	10	$\infty$	1
<i>Palos Verdes</i>	-118.358	33.750	145	10	$\infty$	3

Table 2: Fault model used to subtract the contributions of strike-slip faults to the observed velocities.

Station	East	North	Vertical
CATO	3.2±2.5	8.1±2.6	-0.4± 9.9
CSUN	-3.5±8.3	-1.6±4.0	15.4±11.8
HAP2	-8.6±2.8	6.9±3.0	-2.4±19.4
HAPY	-13.7±7.7	0.3±5.0	-2.6±22.3
LNCH	12.2±2.2	-5.1±2.4	62.8±11.8
OATT	-2.2±2.0	4.6±2.1	20.8± 6.3
SAFE	-6.1±1.9	4.2±2.0	23.4± 4.4

Table 3: Station velocities used for the inversions. The shear model has been removed from the horizontal velocities. The vertical velocities are unchanged. Errors are  $1\sigma$ .

Parameter	One Fault	Two Faults	
		Main Plane	Auxiliary Plane
x (km)	-8±2	-10± 2	-29± 6
y (km)	11±3	6± 4	4± 6
strike	120°	120°	103°± 6°
dip	40°	40°	39°±24°
depth (km)	9±3	19± 6	12± 3
width (km)	9±3	20± 7	18± 5
length (km)	13	12± 3	21
strike-slip (mm/yr)	40±17	20±22	-28± 9
dip-slip (mm/yr)	142±28	217±28	43±12

Table 4: Fault parameters for one and two fault inversions.  $\chi^2/\text{dof} = 2.2$  for the one-fault inversion and  $\chi^2/\text{dof} = 1.5$  for the two-fault inversion. Errors are estimates for the two fault model which is poorly constrained. Parameters with no error given were fixed for these cases. The length of the auxiliary plane was originally solved for, but the error was poorly determined. The x and y coordinates are distances from the epicenter of the Northridge earthquake (N34.20883, W118.54067) in east and north respectively. These models are representative and the errors ( $1\sigma$ ) are probably optimistic, particularly for the auxiliary plane which represents deformation in that region.

## Figures

Figure 1: Post-Northridge GPS network. The square patch shows the approximate projection of the rupture plane onto the surface. The epicenter of the earthquake is marked by the star. Dashed and dotted lines mark major and minor fault traces. The Ventura basin is marked by the hachured region.

Figure 2: Time series for the stations used in this analysis. Errors are scaled  $1\sigma$ .

Figure 3: Vertical time series for the station Lynch (LNCH) located in the Granada Hills near the upper part of the mainshock rupture plane. The log fit is the function  $y=51.1 \cdot \log(t-t_0)+57.18$  and the exponential fit is the function  $y=110.8 \cdot (1-\exp(-1.5 \cdot (t-t_0)))-46.78$ , where  $t_0$  is the time of the earthquake.

Figure 4: Calculated displacements from the Northridge aftershock sequence excluding aftershocks occurring on January 17, 1994 and the M 5.1 January 29, 1994 aftershock. The post-seismic GPS station velocities are for displacement in mm after one year and are plotted with  $1\sigma$  error ellipses. The predicted displacements for the stations (bold arrows) and the general displacement field for the region from the aftershocks are also shown.

Figure 5: Observations (with ellipses) and modeled velocities (bold arrows) for the one-fault model. Error ellipses represent  $1\sigma$ . The shaded area marks the projection of the modeled fault onto the surface.

Figure 6: Cross-section of rupture plane, modeled fault, and stations projected onto a N30°E plane for the one-fault model.

Figure 7: Observations and modeled velocities for the two-fault model. Error ellipses represent  $1\sigma$ . The shaded area marks the projection of the modeled fault onto the surface.

Figure 8: Cross-section of rupture plane, modeled faults, and stations projected onto a N30°E plane for the two-fault model. Note that the auxiliary plane strikes N77°W. The eastern edge of the auxiliary plane is projected onto the figure.

Figure 9: North-south profile of observed and modeled vertical velocities for the 1.5 year period following the mainshock. The values are projected onto the plane oriented N30°E.

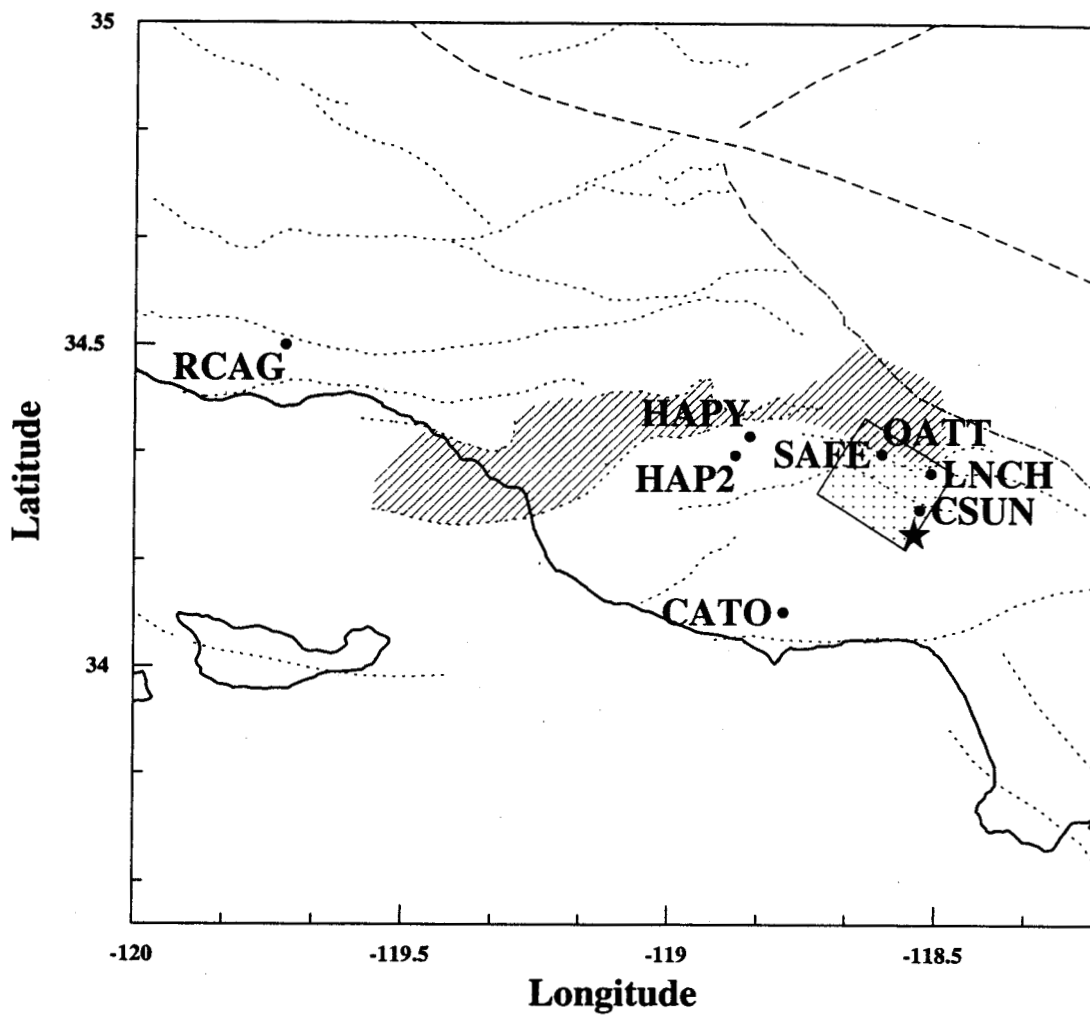


Figure 1

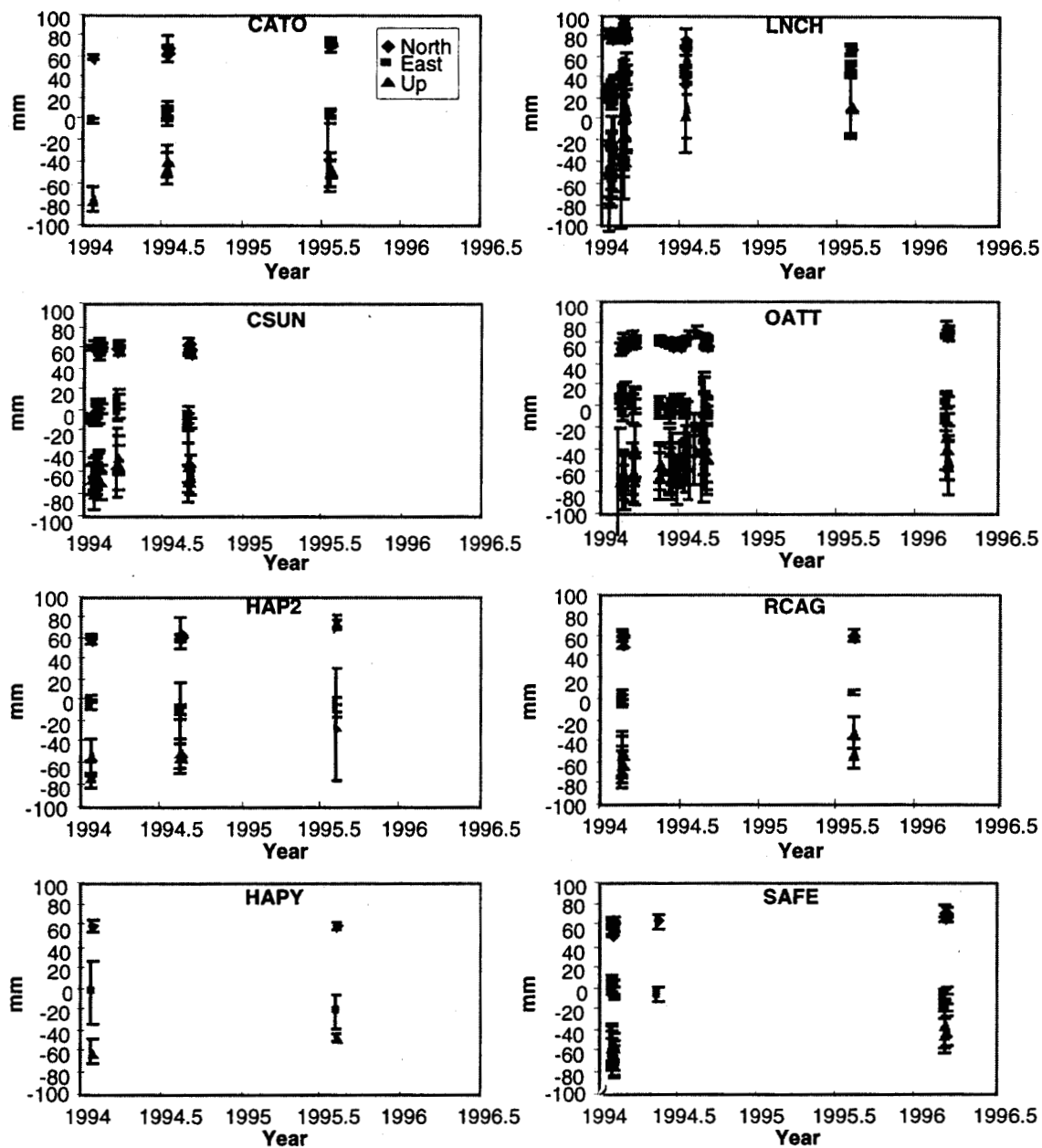


Figure 2

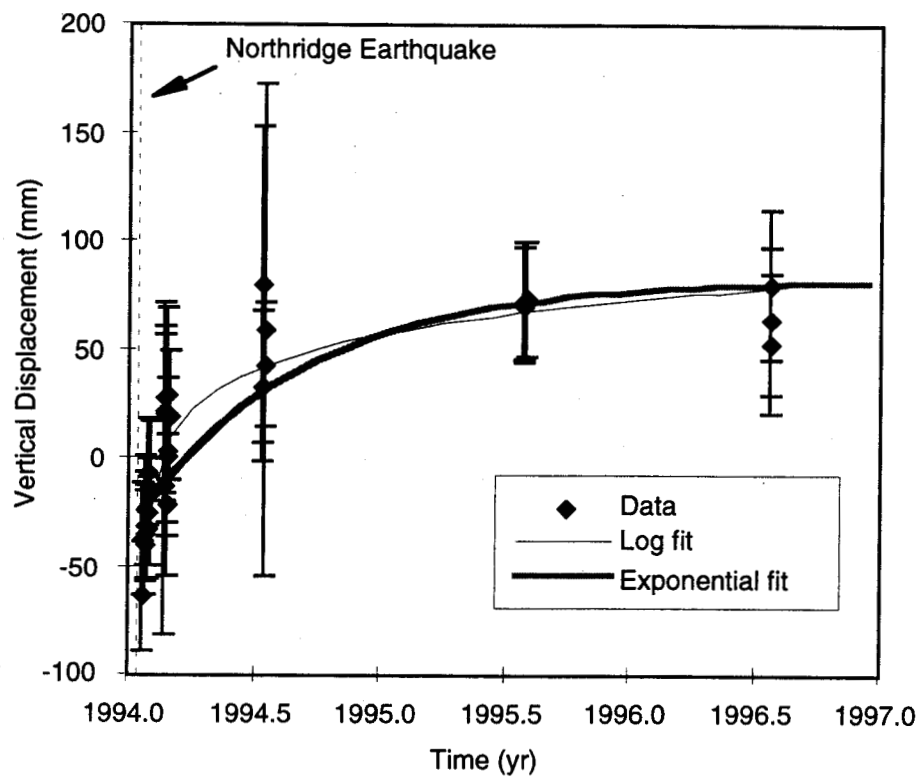


Figure 3

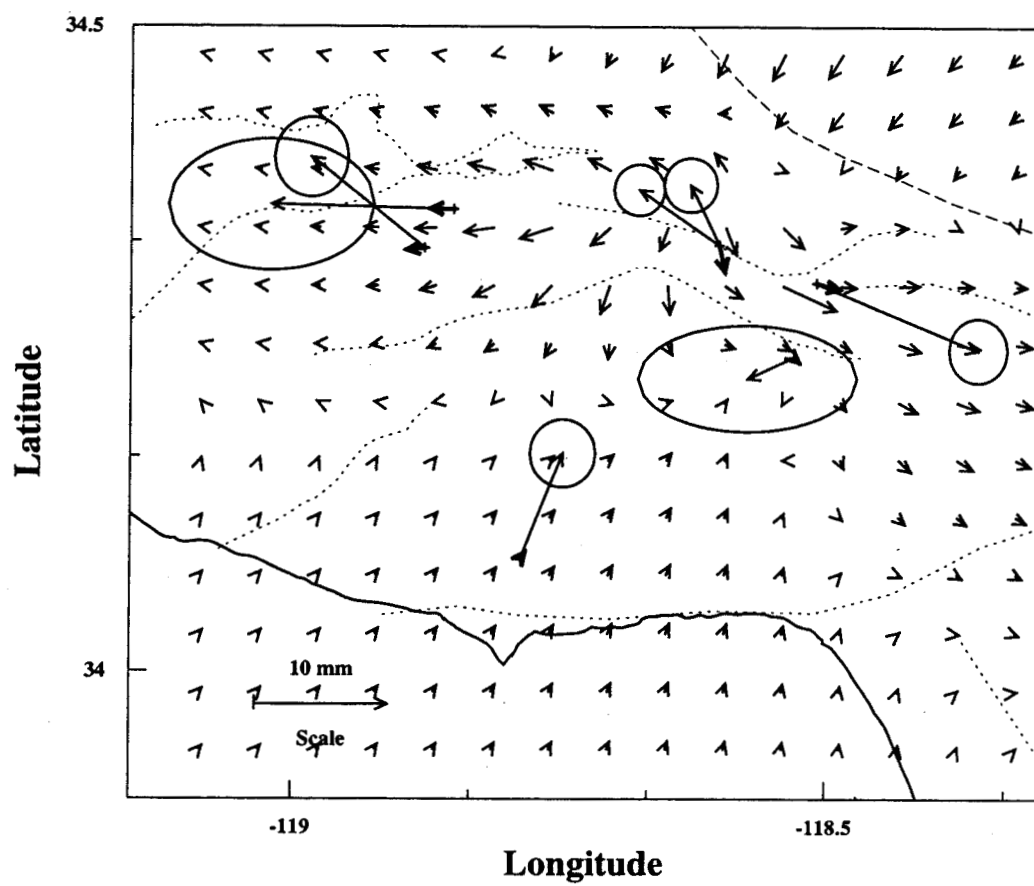


Figure 4

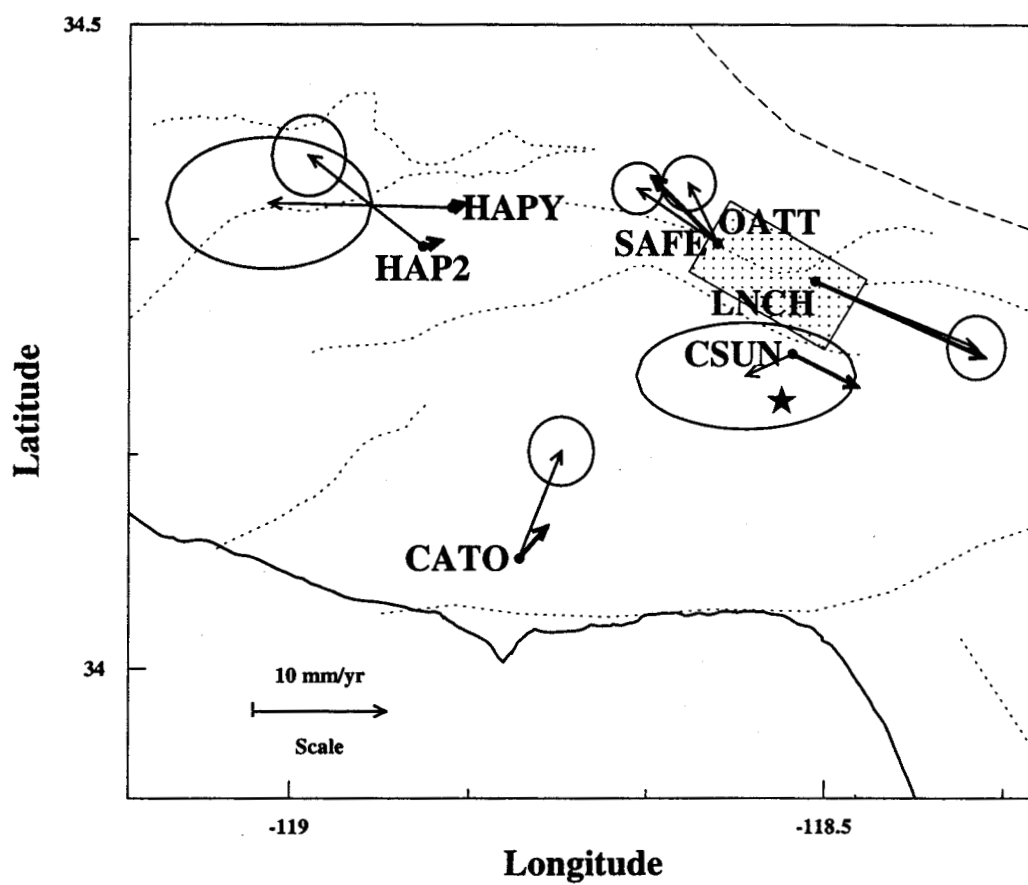


Figure 5

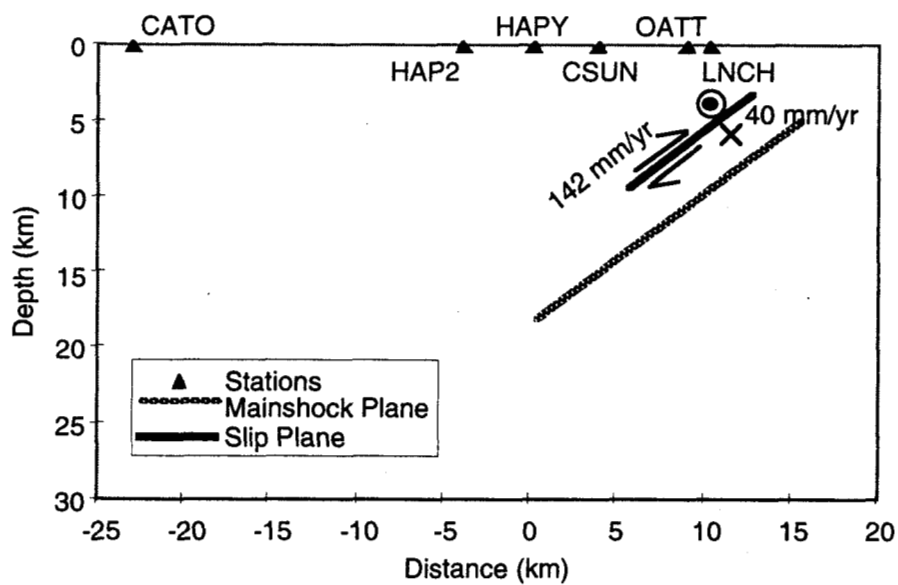


Figure 6

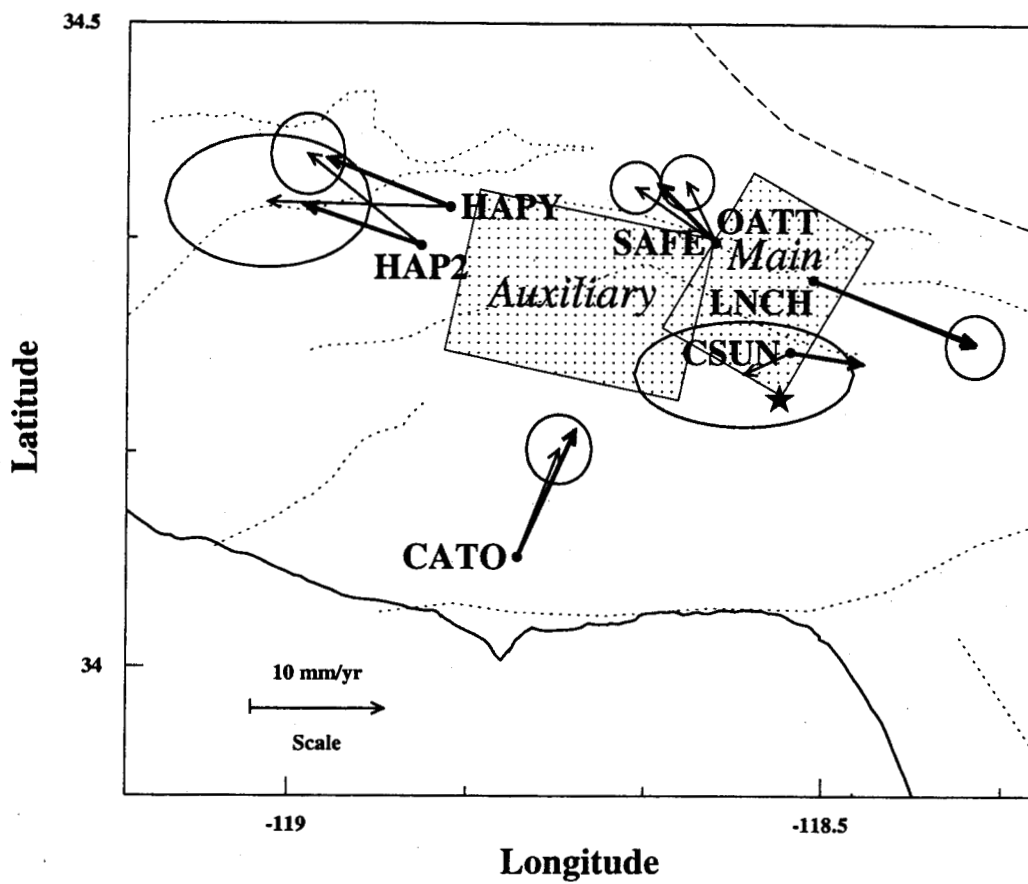


Figure 7

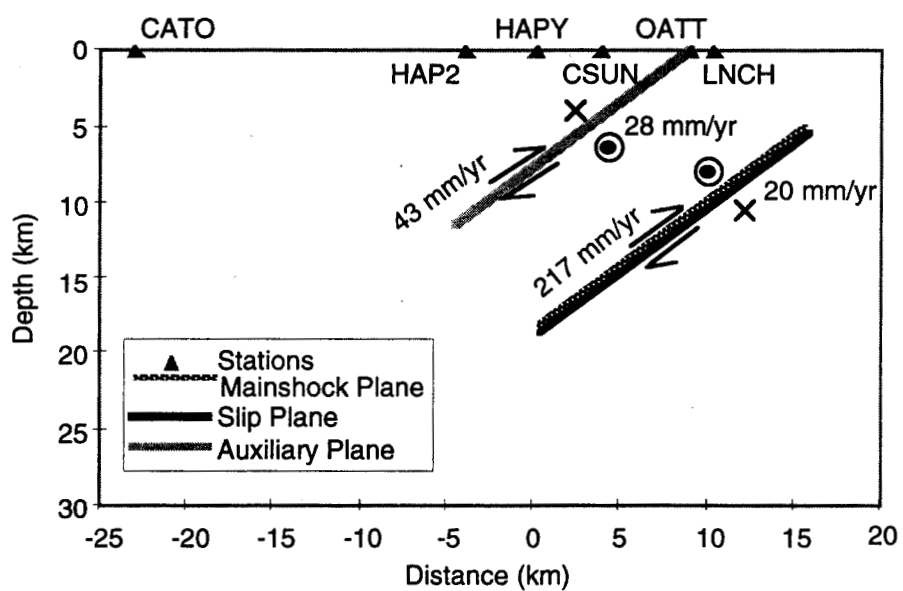


Figure 8

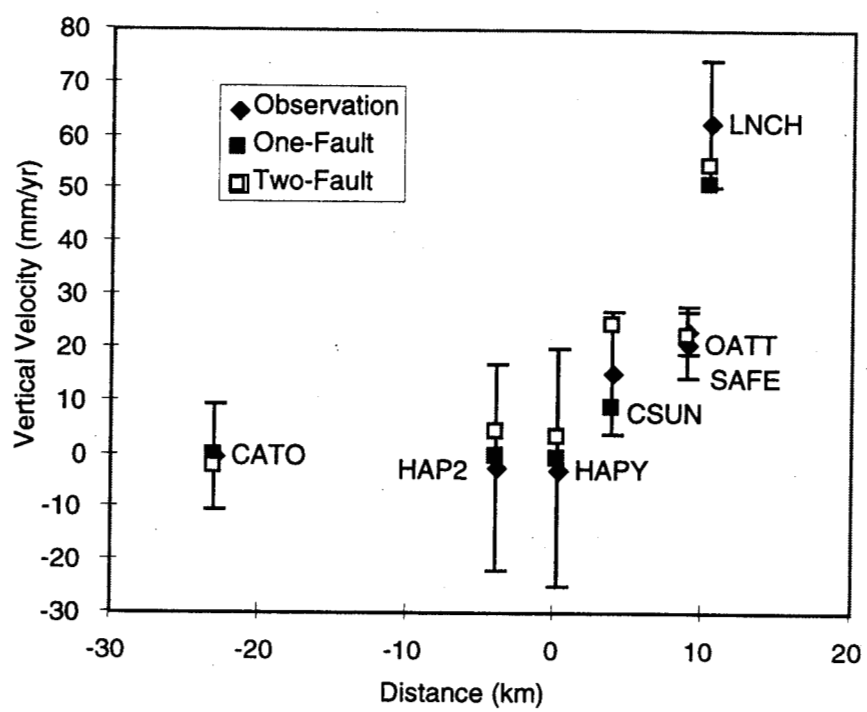


Figure 9